Article

Optofluidic Encapsulation of Crystalline Colloidal Arrays into Spherical Membrane

Shin-Hyun Kim, Seog-Jin Jeon, and Seung-Man Yang

J. Am. Chem. Soc., **2008**, 130 (18), 6040-6046 • DOI: 10.1021/ja800844w • Publication Date (Web): 08 April 2008

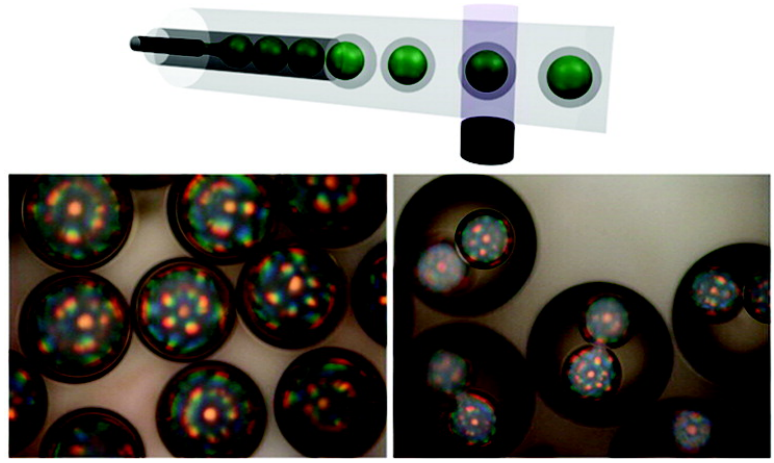

J|A|C|S
ARTICLES

Published on Web 04/08/2008

Optofluidic Encapsulation of Crystalline Colloidal Arrays into Spherical Membrane

Shin-Hyun Kim, Seog-Jin Jeon, and Seung-Man Yang*

National Creative Research Initiative Center for Integrated Optofluidic Systems and Department of Chemical and Biomolecular Engineering, Korea Advanced Institute of Science and Technology, Daejeon, 305-701 Korea

Received February 11, 2008; E-mail: smyang@kaist.ac.kr

Abstract: Double emulsion droplets encapsulating crystalline colloidal arrays (CCAs) with a narrow size distribution were produced using an optofluidic device. The shell phase of the double emulsion was a photocurable resin that was photopolymerized downstream of the fluidic channel within 1 s after drop generation. The present optofluidic synthesis scheme was very effective for fabricating highly monodisperse spherical CCAs that were made structurally stable by *in situ* photopolymerization of the encapsulating shells. The shell thickness and the number of core emulsion drops could be controlled by varying the flow rates of the three coflowing streams in the dripping regime. The spherical CCAs confined in the shell exhibited distinct diffraction patterns in the visible range, in contrast to conventional film-type CCAs. As a result of their structure, the spherical CCAs exhibited photonic band gaps for normal incident light independent of the position on the spherical surface. This property was induced by heterogeneous nucleation at the smooth wall of the spherical emulsion drop during crystallization into a face-centered cubic (fcc) structure. On the other hand, the solidified shells did not permit the penetration of ionic species, enabling the CCAs to maintain their structure in a continuous aqueous phase of high ionic strength for at least 1 month. In addition, the evaporation of water molecules inside the shell was slowed considerably when the core–shell microparticles were exposed to air: It took approximately 6 h for a suspension encapsulated in a thick shell to evaporate completely, which is ~1000 times longer than the evaporation time for water droplets with the same volume. Finally, the spherical CCAs additionally exhibited enhanced stability against external electric fields. The spherical geometry and high dielectric constant of the suspension contributed to reducing the electric field inside the shell, thereby inhibiting the electrophoretic movement of the charged particles.

Introduction

The phase behavior of charged colloidal particles has attracted much attention in materials chemistry and soft condensed-matter physics. Because such colloids take on various crystalline structures depending on the volume fraction and strength of the repulsive interparticle potential, they are used as models of atomic and molecular systems.[1–3] Recently, Bartlett et al.[4] and Leunissen et al.[5] showed experimentally and theoretically that unconventional crystal structures such as CsCl, NaCl, and assemblies of bimodal colloids can be reproduced using bidisperse colloidal systems with oppositely charged particles. Meanwhile, the periodic modulation of refractive index by crystalline colloidal arrays (CCAs) gives rise to photonic band gaps and to a sparkling gem-like appearance.[6] Compared with dried colloidal crystals prepared by evaporation-induced self-assembly, CCAs are formed rapidly with low defect densities. However, CCAs are fragile under external disturbances because the colloidal particles are not closely packed in a liquid medium. To improve the stability of CCAs, Asher et al. developed polymerized CCAs (PCCAs), which are CCAs locked with a hydrogel network.[7] In particular, the lattice constant of PCCAs can be varied dynamically by swelling or contracting the hydrogel, enabling tuning of the photonic band gap. By exploiting this property, PCCAs have been used as effective detectors for specific biomolecules by introducing biological probes into the hydrogel network.[8] Lawrence et al. showed the emission inhibition of dye molecules in a PCCA matrix at a stop band[9] and fabricated an organic laser using a PCCA as a tunable mirror.[10]

Fabricating CCAs with a spherical or cylindrical geometry is of particular interest because colloidal crystals with these geometries possess photonic band gaps for normal incident light independent of the position on the crystal surface, a property that stands in contrast to the anisotropies of the band gaps with respect to the incident angle of light upon conventional CCA

(1) Monovoukas, Y.; Gast, A. P. *J. Colloid Interface Sci.* **1989**, *128*, 533–548.
(2) Kegel, W. K.; van Blaaderen, A. *Science* **2000**, *287*, 290–293.
(3) Yethiraj, A.; van Blaaderen, A. *Nature* **2003**, *421*, 513–517.
(4) Bartlett, P.; Campbell, A. I. *Phys. Rev. Lett.* **2005**, *95*, 128302.
(5) Leunissen, M. E.; Christova, C. G.; Hynninen, A. P.; Royall, C. P.; Campbell, A. I.; Imhof, A.; Dijkstra, M.; van Roij, R.; van Blaaderen, A. *Nature* **2005**, *437*, 235–240.
(6) Rundquist, P. A.; Photinos, P.; Jagannathan, S.; Asher, S. A. *J. Chem. Phys.* **1989**, *91*, 4932–4941.
(7) Asher, S. A.; Holtz, J.; Liu, L.; Wu, Z. *J. Am. Chem. Soc.* **1994**, *116*, 4997–4998.
(8) Holtz, J.; Asher, S. A. *Nature* **1997**, *389*, 829–832.
(9) Lawrence, J. R.; Ying, Y.; Shim, G. H.; Jiang, P.; Han, M. G.; Ying, Y.; Foulger, S. H. *Adv. Mater.* **2005**, *17*, 2344–2349.
(10) Lawrence, J. R.; Ying, Y.; Jiang, P.; Foulger, S. H. *Adv. Mater.* **2006**, *18*, 300–303.

10.1021/ja800844w CCC: $40.75

films.[11–15] However, spherical or cylindrical CCAs have yet to be fabricated on account of the low stability of such crystals. In addition, encapsulation of a CCA in a liquid phase presents challenges in regard to generating a tunable color pigment with a fast response. Although PCCAs have tunable band gaps and a high stability, the color tuning is too slow for PCCAs to be used as color pigments due to the viscoelastic behavior of the hydrogel network.

Recent developments in microfluidics have enabled the continuous preparation of anisotropic or functional microparticles by emulsion polymerization. A few representative examples are plug and disk-type particles by using the shape of flow channel as a template,[16] microparticles doped with dye molecules or quantum dots,[17] capsules by interfacial polymerization from simple emulsions, [18,19] and Janus particles with anisotropic optical or electrical properties from biphase emulsions or bubbles.[20–24] In particular, monodisperse single or double emulsion droplets have been produced in a controlled manner via one-step or two-step drop breakup in microfluidic devices.[25–30] Also, Utada et al.[26] reported that vesicle structures have been fabricated by introducing a block copolymer into the middle phase of a double emulsion, and Nie et al.[27a] prepared various types of polymeric particles by photopolymerization of double emulsion droplets. Recently, Kim et al.[29a] fabricated the thermoresponsive microgel shells using double emulsion droplets produced in a microfluidic device.

In this article, we demonstrate the optofluidic encapsulation of CCAs using a double emulsion with a photocurable middle phase. The optofluidic encapsulation of CCAs produced highly monodisperse spherical CCAs with all identical core structures in a controlled manner. In particular, the spherical CCAs gained structural stability immediately after they were produced by *in situ* photoinduced polymerization of the encapsulating shells. Because CCAs tend to lose stability in an aqueous phase containing ions and other impurities or in an electric field, encapsulation of a CCA with a spherical shell of low permeabilities of ions and molecules can afford long-time stability to the CCA. In addition, the shell inhibits evaporation of water molecules even when the encapsulated CCA is exposed to the atmosphere. More importantly, spherical CCAs show different optical properties from conventional film-type CCAs because the densest plane of the fcc structure, the (111) plane, is the entire spherical inner wall of the shell.[31]

In the subsequent sections, we first describe the fabrication of double emulsions containing a CCA suspension as a core and a photocurable oil as a shell phase using a microcapillary device. Then, we discuss the origin of the diffraction patterns of spherical CCAs through a comparison with cylindrical and conventional film-type CCAs. Finally, we examine the spherical shell properties associated with the permeability of the shell to impurities and water molecules, and finally we consider the electric field distribution within the encapsulated CCA structure to confirm the phase stability of CCAs under an electric field. The external electric or magnetic field can modulate the lattice constant of the encapsulated CCA and thereby change the diffraction colors, which is relevant to its practical application as externally tunable color pigments for reflection-mode display.

Preparation of Encapsulated Spherical Crystalline Colloidal Arrays (SCCAs) with a Polymeric Shell. The simple generation of emulsions with controlled size and rate of production has been successfully achieved using continuous drop breakup in microfluidic devices with T-junction channels or capillary tubes with micron-sized diameters. Recently, more complex geometries of channels or microtubes have been developed for additional flexibility in the generation of multiphase emulsions. In this study, we used a sequential droplet break-off technique in coaxial and coflowing streams in glass microcapillary tubes to prepare a double emulsion, as shown schematically in Figure 1a. The mode of drop breakup in similar coflowing devices was used for preparing monodisperse water-in-oil drops which contained colloidal particles.[25c] Here, the glass capillary device was composed of inner, middle, and outer capillaries with diameters of 150, 280, and 400 μm, respectively, and the distance between the tips of the inner and middle capillaries was 5 mm. Using this system, the diameters of the core and shell emulsion droplets could be controlled by varying the inner diameters of the capillaries and the flow rates of the coflowing streams. Here, an aqueous suspension of polystyrene particles (328 nm in diameter; 10 vol.% in particle loading) moved through the inner capillary, and a photocurable ethoxylated trimethylolpropane triacrylate (ETPTA) resin was forced to flow through the middle capillary together with 0.2 wt % 2-hydroxy-2-methyl-1-phenyl-1-propanone as photoinitiator and 2 wt % surfactant sorbitan monooleate (SPAN 80; Aldrich, denoted as surfactant 2) for stabilizing the water-in-oil emulsion. The aqueous outer flow contained a 1 wt % surfactant ethyleneoxide−propyleneoxide−ethyleneoxide triblock copoly-

(11) Velev, O. D.; Lenhoff, A. M.; Kaler, E. W. *Science* **2000**, *287*, 2240–2243.
(12) Moon, J. H.; Yi, G.-R.; Yang, S.-M.; Pine, D. J.; Park, S. B. *Adv. Mater.* **2004**, *16*, 605–609.
(13) Kim, S.-H.; Lee, S. Y.; Yi, G.-R.; Pine, D. J.; Yang, S.-M. *J. Am. Chem. Soc.* **2006**, *128*, 10897–10904.
(14) Moon, J. H.; Kim, S.; Yi, G.-R.; Lee, Y.-H.; Yang, S.-M. *Langmuir* **2004**, *20*, 2033–2035.
(15) Kamp, U.; Kitaev, V.; von Freymann, G.; Ozin, G. A.; Mabury, S. A. *Adv. Mater.* **2005**, *17*, 438–443.
(16) Dendukuri, D.; Tsoi, K.; Hatton, T. A.; Doyle, P. S. *Langmuir* **2005**, *21*, 2113–2116.
(17) Xu, S.; Nie, Z.; Seo, M.; Lewis, P.; Kumacheva, E.; Stone, H. A.; Garstecki, P.; Weibel, D. B.; Gitlin, I.; Whitesides, G. M. *Angew. Chem., Int. Ed.* **2005**, *44*, 724–728.
(18) Takeuchi, S.; Garstecki, P.; Weibel, D. B.; Whitesides, G. M. *Adv. Mater.* **2005**, *17*, 1067–1072.
(19) Quevedo, E.; Steinbacher, J.; McQuade, D. T. *J. Am. Chem. Soc.* **2005**, *127*, 10498–10499.
(20) Nisisako, T.; Torii, T.; Takahashi, T.; Takizawa, Y. *Adv. Mater.* **2006**, *18*, 1152–1156.
(21) Nisisako, T.; Torii, T. *Lab Chip* **2008**, *8*, 287–293.
(22) Nie, Z.; Li, W.; Seo, M.; Xu, S.; Kumacheva, E. *J. Am. Chem. Soc.* **2006**, *128*, 9408–9412.
(23) Shepherd, R. F.; Conrad, J. C.; Rhodes, S. K.; Link, D. R.; Marquez, M.; Weitz, D. A.; Lewis, J. A. *Langmuir* **2006**, *22*, 8618–8622.
(24) Subramanian, A. B.; Abkarian, M.; Stone, H. A. *Nat. Mater.* **2005**, *4*, 553–556.
(25) (a) Okushima, S.; Nisisako, T.; Torii, T.; Higuchi, T. *Langmuir* **2004**, *20*, 9905–9908. (b) Nisisako, T.; Okushima, S.; Torii, T. *Soft Matter* **2005**, *1*, 23–27. (c) Yi, G.-R.; Manoharan, V. N.; Klein, S.; Brzezinska, K. R.; Pine, D. J.; Lange, F. F.; Yang, S.-M. *Adv. Mater.* **2002**, *14*, 1137–1140.
(26) Utada, A. S.; Lorenceau, E.; Link, D. R.; Kaplan, P. D.; Stone, H. A.; Weitz, D. A. *Science* **2005**, *308*, 537–541.
(27) (a) Nie, Z.; Xu, S.; Seo, M.; Lewis, P. C.; Kumacheva, E. *J. Am. Chem. Soc.* **2005**, *127*, 8058–8063. (b) Seo, M.; Paquet, C.; Nie, Z.; Xu, S.; Kumacheva, E. *Soft Matter* **2007**, *3*, 986–992.
(28) Lorenceau, E.; Utada, A. S.; Link, D. R.; Cristobal, G.; Joanicot, M.; Weitz, D. A. *Langmuir* **2005**, *21*, 9138–9186.
(29) (a) Kim, J.-W.; Utada, A. S.; Fernandez-Nieves, A.; Hu, Z.; Weitz, D. A. *Angew. Chem., Int. Ed.* **2007**, *46*, 1819–1822. (b) Chu, L.-Y.; Utada, A. S.; Shah, R. K.; Kim, J.-W.; Weitz, D. A. *Angew. Chem., Int. Ed.* **2007**, *46*, 8970–8974.
(30) Barbier, V.; Tatoulian, M.; Li, H.; Arefi-Khonsari, F.; Ajdari, A.; Tabeling, P. *Langmuir* **2006**, *22*, 5230–5232.
(31) Grier, D. G.; Murray, C. A. *J. Chem. Phys.* **1994**, *100*, 9088–9095.

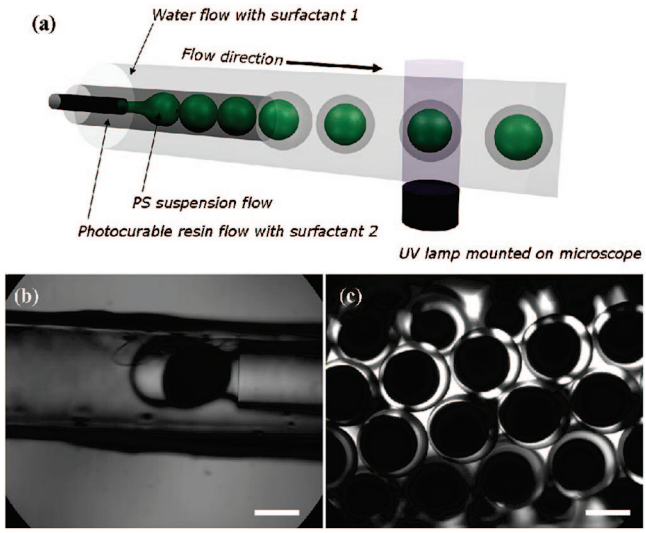

Figure 1. (a) Schematic of optofluidic encapsulation of CCAs with microcapillary device and UV irradiation. Still shot images of (b) double emulsion generation at the end of middle capillary and (c) its flow downstream of outer capillary. The core emulsion looks opaque due to scattering by colloidal particles while shell phase looks transparent. The scale bars in (b) and (c) are 200 μm.

mer (Pluronic F108; BASF, denoted as surfactant 1) as stabilizer for the oil-in-water emulsion. 10 vol. % of 328 nm PS particles can induce the second-order diffraction in the visible range. The PS suspension at a higher concentration would clog the capillary if the suspension is unstable and forms aggregates. Because of the high hydrophilicity of the glass capillaries, we treated the inner surface of the middle capillary with the hydrophobic molecule octadecyltrichlorosilane (OTS) before assembling the tubes. Without this surface modification, the suspension flowed along the hydrophilic surface of the middle capillary and water-in-oil emulsion drops were not able to be generated at the tip of the inner capillary. Typically, to generate a stable double emulsion in the regime of the dripping mode of drop breakup, the flow rates in the inner, middle, and outer capillaries were set at 1, 0.3, and 100 μL/min, respectively. However, the flow rates were changed slightly from these typical settings to control the shell thickness and the number of the encapsulated core emulsion drops. About 1 s later since the drop generation, the shells of the generated double emulsion drops were selectively solidified downstream by UV irradiation from a 100 W mercury lamp for 1 s through a 10× objective lens which was mounted on a microscope. The resulting CCA core-ETPTA shell microparticles were collected in the plastic dish at the tip of the outer capillary. To ensure the complete solidification, the microparticles were exposed again to UV light for 10 s after the microparticles were collected. Figure 1b and 1c show images taken at the tip of the middle capillary and in the downstream region, respectively. Because of scattering by the PS particles, the core emulsion was opaque whereas the shell (ETPTA) was transparent. Movie Clip S1 of the Supporting Information shows the generation of the double emulsion drops at the tip of the middle capillary and their subsequent movement along the flow downstream. After photopolymerization of the shell, the microparticles were washed with water to remove residual surfactant and then observed through an optical microscope in reflection mode. Figure 2a and 2b show images of the prepared core–shell microparticles. The average radius of the microparticles was 170 μm with a coefficient of variation (CV) of 5%, and the shell thickness was ~15 μm. CCAs formed in the core

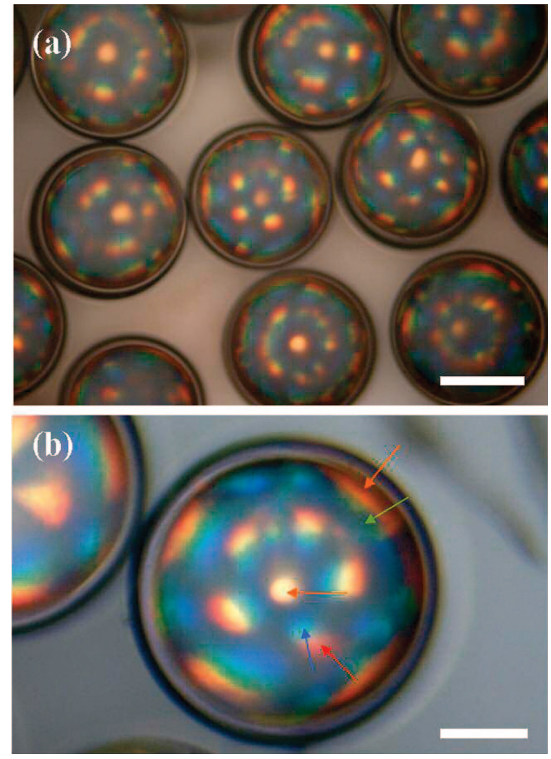

Figure 2. (a) Optical microscope image of SCCAs confined in polymeric shells dispersed in water phase and (b) magnified image of single capsule. We can observe the diffraction colors from SCCAs as denoted by arrows. The scale bars in (a) and (b) are 200 and 100 μm, respectively.

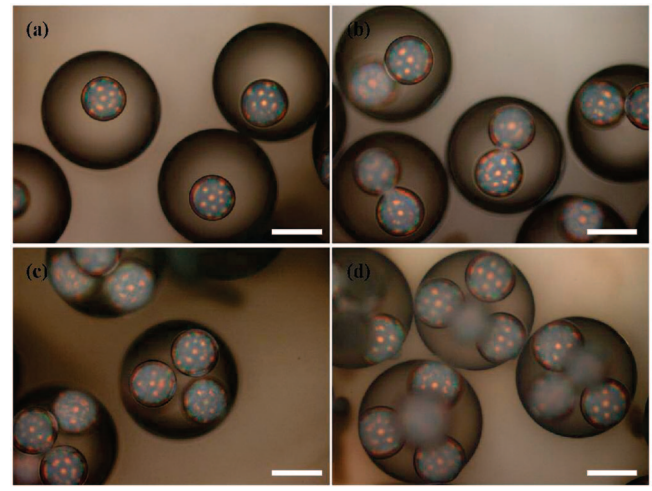

Figure 3. Optical microscope images of the core–shell microparticles with (a) single, (b) dual, (c) triple, and (d) quadruple cores. The scale bars in (a−d) are 200 μm.

emulsion showed the diffraction color patterns and kept the colors for at least 3 months.

By changing the flow rates, we could change the number of small core emulsion drops; for example, Figure 3 shows images of core–shell microparticles with single, double, triple, and quadruple cores. As can be seen in Figure 3, similar diffraction patterns were also observed for the multicore–shell microparticles. In Movie Clip S2 of the Supporting Information, we can clearly see the generation of a double emulsion containing four encapsulated emulsion drops. When a spherical shell was overcrowded with relatively large emulsion drops, the shell could not confine the emulsion drops keeping the spherical

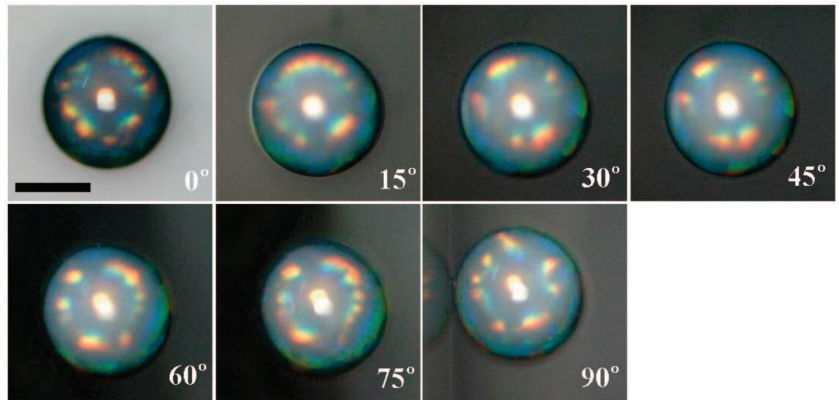

Figure 4. Optical microscope images taken at various angles between observation direction and substrate normal. All images show similar diffraction color patterns. The scale bar is 200 μm.

shape. In this case, the shell and core emulsion drops were deformed confining the core emulsion drops within the thin shell layer (see the Figure S1 of the Supporting Information). This behavior indicates that the surfactant molecules stabilized effectively both the interfaces and immediate UV irradiation after drop break-off solidified the thinning shell before bursting of the core emulsion drops. Without *in situ* solidification of the shell, the emulsion drops burst out into the continuous phase and the edge of the ruptured shell had the form of a very thin layer with a thickness on the order of 100 nm.

Crystal Structures and Diffraction Colors of SCCA. As we described previously, the reflection spectrum of a spherical colloidal crystal (photonic ball) remains unchanged when the crystal is rotated under light impinging on the crystal surface at a fixed incident angle. This characteristic arises because the entire surface of the photonic ball has a (111) lattice symmetry of an fcc structure, which is induced by the heterogeneous nucleation on the smooth wall of the spherical emulsion drop during crystallization. We confirmed this property by observing the single SCCA encapsulated by the ETPTA shell from various angles. To achieve this, the surrounding water was removed and the core–shell microparticle, in which 328 nm PS particles were dispersed in the core emulsion drop, was placed on a glass substrate. As seen in Figure 4, the diffraction patterns were similar for all angles ranging from 0° to 90°. In particular, a bright reddish dot at the center of the microparticle is evident in all images; this dot corresponds to the second-order Bragg diffraction from the stacked (111) planes. These findings thus indicate that the entire surface of the core is composed of hexagonal arrays of PS colloidal particles. All of the SCCAs prepared in the present study showed reddish and bluish spots or short lines near the area between the center and edge, as observed in Figures 2, 3, and 4. In addition, the edge region showed reddish and greenish spots or lines for SCCAs dispersed in water (Figures 2 and 3), which were not observed for SCCAs in air (Figure 4). This is because the refractive index contrast between air and ETPTA is large so that there is negligible reflection in the direction of observation.

To find the origin of these color diffraction patterns, we additionally prepared a cylindrical CCA by infiltrating the aqueous suspension of 328 nm PS beads into a glass capillary of diameter 230 μm. To reduce the refractive index contrast between air and glass, we form a thin water film outside the capillary and observed the diffraction pattern from the cylinder. The cylindrical CCA showed a line that was reddish at the center, reddish and bluish in the middle, and reddish and

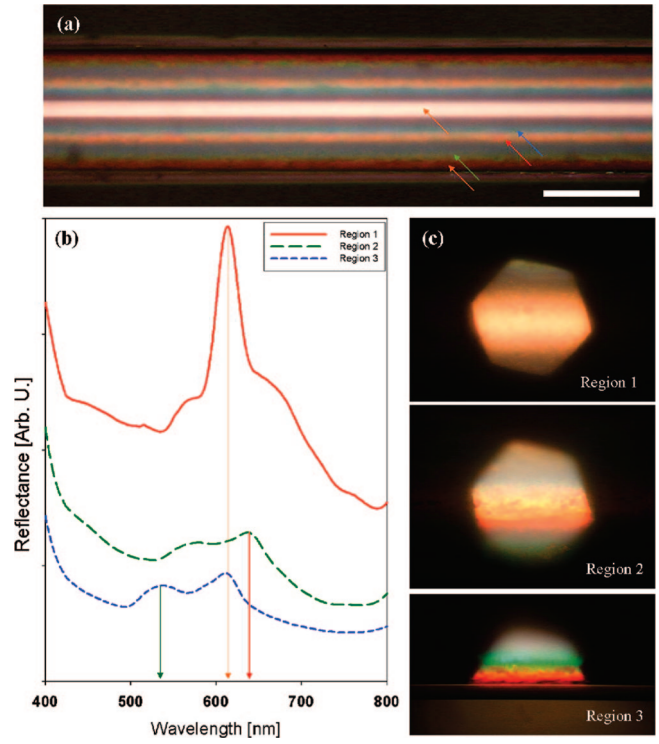

Figure 5. (a) Optical microscope image of cylindrical CCA fabricated by infiltration of the colloidal suspension into the glass capillary. We can observe the diffraction colors from cylindrical CCAs as denoted by arrows. (b) Reflectance spectra from the selected regions of cylindrical CCAs. Three curves are corresponding to reflections from the central area (region 1), middle area between center and edge (region 2), and edge area (region 3) of cylinder. (c) Optical microscope images of corresponding three regions. To collect the light from selected regions, we used field stop and 10× objective lens. The scale bar in (a) is 200 μm.

greenish at the edge, as denoted by arrows in Figure 5a. The transversal distribution of diffraction colors of the cylindrical CCA is similar to the radial distribution of the SCCA. To clarify the origin of similar diffraction patterns, we prepared large cylindrical CCAs of 1 mm in diameter and measured the reflectance spectrum from a local area of the cylindrical CCAs. To achieve this, we used a field stop and a 10× objective lens to collect light from the desired region. The resulting spectra are shown in Figure 5b along with images (c) of each region. As expected from Bragg's law for normal incident light onto a (111) plane, the center region (denoted as region 1) showed a reddish color of wavelength 613 nm. The reflection wavelength

Table 1. Diffraction Wavelengths and Angles between Diffracting Crystal Planes and (111) Plane of fcc Lattice

Plane	Angle	L=1	L=2
(2 0 0)	54.73561	1061.734	530.8671
(0 2 0)	54.73561	1061.734	530.8671
(0 0 2)	54.73561	1061.734	530.8671
(2 2 0)	35.26439	750.7595	375.3797
(2 0 2)	35.26439	750.7595	375.3797
(0 2 2)	35.26439	750.7595	375.3797
(3 1 1)	29.49621	640.2498	320.1249
(1 3 1)	29.49621	640.2498	320.1249
(1 1 3)	29.49621	640.2498	320.1249
(1 1 -1)	70.52878	1225.985	612.9925
(1 -1 1)	70.52878	1225.985	612.9925
(1 -1 -1)	109.4712	1225.985	612.9925
(3 1 -1)	58.51785	640.2498	320.1249
(3 -1 1)	58.51785	640.2498	320.1249
(1 3 -1)	58.51785	640.2498	320.1249
(1 -1 3)	58.51785	640.2498	320.1249
(1 -1 -3)	121.4822	640.2498	320.1249
(1 -3 -1)	121.4822	640.2498	320.1249
(3 -1 -1)	79.97501	640.2498	320.1249
(1 1 -3)	100.025	640.2498	320.1249
(1 -3 1)	100.025	640.2498	320.1249

for the (111) plane depends on the particle diameter D, the refractive indices of the particles and medium, n_p and n_m, respectively, the volume fraction of particles φ, and the incident angle θ:

$$L\lambda = 2dn_{\text{eff}} = \left(\frac{\pi}{3\sqrt{2}\varphi}\right)^{1/3}\left(\frac{8}{3}\right)^{1/2} D\left(n_p^2\varphi + n_m^2(1-\varphi) - \sin^2\theta\right)^{1/2} \quad (1)$$

where L is the diffraction order, and the nearest-neighbor interparticle distance is assumed to be constant at a given volume fraction. Because first-order diffraction induces reflections in the infrared range, we could only observe the second-order diffraction color in the visible range. The middle region (region 2) exhibited a reddish color of wavelength 638 nm at $0.47R$ ($\sim$28°) from the center, where R is the radius of the glass capillary. Although a bluish color was observed in the optical microscope image (Figure 5a), the spectrum does not show this color due to its low intensity. On the other hand, the edge region (region 3) showed a greenish color of wavelength 535 nm at $0.78R$ ($\sim$51°) and a reddish color of wavelength 612 nm at $0.93R$ ($\sim$68°). The wavelength and position of each color were consistent with the diffraction wavelength and angle relative to a typical plane of the fcc structure. The first and second order diffraction wavelengths and angles between the diffracting crystal planes and the (111) plane of an fcc lattice are summarized in Table 1. The diffraction wavelengths were calculated using Bragg's law assuming a volume fraction of 0.109, which is the value that satisfies eq 1 under conditions of reflection from the center. Because the entire surface of the cylindrical CCA has a (111) plane, the position of the colored area can be interpreted as the angle between the observation and [111] directions by simple geometrical considerations. By comparing the angles and wavelengths from Table 1, we find that the reddish color in region 2 corresponds to the diffraction from the (311), (131), and (113) planes, while the greenish and reddish colors in region 3 correspond to diffraction from the (200), (020), and (002) planes and (11–1), (1–11), and (1–1 −1) planes, respectively. Small deviations are observed between the observed colors and predicted diffraction behavior, which we attribute to the refraction of the incident and reflected beams by the curved glass surface.

The diffraction colors appear as lines in the cylindrical CCA but as dots or short lines in the SCCA pattern. This difference can be attributed to the characteristics of the spherical surface versus the cylindrical surface, i.e., the curvatures of spherical and cylindrical surfaces. At every point on a spherical surface, the principal curvatures are the same and equal to $1/R$ in which R is the radius of the sphere. Therefore, any normal plane cuts the spherical surface in a plane curve which is a "convex" circle. These geometrical features create inevitably defects in the hexagonal arrangement of colloidal particles on a spherical surface.[32,33] In particular, large system sizes such as in the case of the SCCAs examined in this study always induce "scars" on the spherical surface, which correspond to repetitive chains of 5-fold and 7-fold defects, to reduce the stress. As a result, the crystalline direction may differ across the surface of the sphere, although the surface normal is always the [111] direction. This random crystal orientation induces diffraction patterns comprised of dots or short lines. However, at a point on a cylindrical surface, the principal curvatures are different: one is $1/R$ and the other is zero, in which R is the radius of the cylinder. Therefore, on a cylindrical surface, any plane curve on a transverse normal plane is a "convex" circle whereas a plane curve on a longitudinal normal plane is a straight line. The *convex* curvature in the transversal principal plane of the cylindrical CCA is responsible for the transversal distribution of diffraction colors which is similar to the radial distribution of the SCCA. On the other hand, due to the existence of the zero principal curvature, the curved surface of the cylinder can accept the hexagonal colloidal arrays without defects by bending the flat (111) plane, similar to the armchair (n, n) structure of carbon nanotubes. Consequently the cylindrical CCAs show line patterns along the longitudinal direction, which is in contrast with the diffraction patterns of dots or short lines on the spherical CCA.

Obviously, for a flat film-type CCA which has zero principal curvatures everywhere, the densest (111) plane of fcc can be formed over the surface with no defects. Therefore, the characteristic spots or lines, marked by arrows in Figure 2b or Figure 5a, are not observed and the diffraction color is uniform in the conventional film-type CCA (see Figure S2 of the Supporting Information. Herein, we prepared the CCA film by infiltration of the same suspension between two slide glasses separated by 50 μm.)

For the spherical and cylindrical CCAs, of which both of the first-order diffractions are in the visible range, we used the aqueous suspension of smaller PS beads of 165 nm in diameter.

(32) Bausch, A. R.; Bowick, M. J.; Cacciuto, A.; Dinsmore, A. D.; Hsu, M. F.; Nelson, D. R.; Nikolaides, M. G.; Travesset, A.; Weitz, D. A. *Science* **2003**, *299*, 1716–1718.
(33) Einert, T.; Lipowsky, P.; Schilling, J.; Bowick, M. J.; Bausch, A. R. *Langmuir* **2005**, *21*, 12076–12079.
(34) (a) Ge, J.; Hu, Y.; Biasini, M.; Beyermann, W. P.; Yin, Y. *Angew. Chem., Int. Ed.* **2007**, *46*, 4342–4345. (b) Ge, J.; Hu, Y.; Yin, Y. *Angew. Chem., Int. Ed.* **2007**, *46*, 7428–7431.

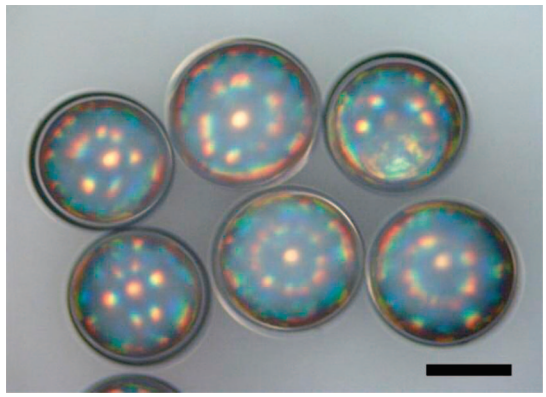

Figure 6. Optical microscope image of SCCAs dispersed in 0.1 M sodium chloride (NaCl) solution for 1 month. Ionic impurities cannot penetrate through the ETPTA shells. The scale bar is 200 μm.

As shown in Figure S3 of the Supporting Information, the CCAs showed a bright first-order reflection at the center region arising from the (111) plane and the same color at the edge region due to the (11–1), (1–11), (1–1–1) planes. These CCAs exhibit simple diffraction patterns rather than the complex color patterns observed above for the second-order diffraction because the first-order diffraction induced by the {111} family of planes is very strong, compared with diffraction from other planes.

Properties of ETPTA-Encapsulated SCCAs. Usually, PS particles are made stable in an aqueous medium by anchoring functional groups on their surfaces. However, the particles can be destabilized by increasing the ionic strength of the medium and consequently reducing the electrostatic repulsions. Indeed, when we added 5 μL of 0.1 M sodium chloride (NaCl) solution to 1 mL of CCA suspension, the diffraction color disappeared immediately due to the destabilization-induced loss of crystalline structure. To test the permeability of the ETPTA shell to sodium ions, we dispersed the microparticles comprised of CCA cores and ETPTA shells in 0.1 M NaCl solution for 1 month. The ETPTA shells with micrometer scale thicknesses were able to block out the ion transfer through the shells, keeping the CCA suspension stable with the diffraction colors of the core–shell particles remaining unchanged, as shown in Figure 6.

The permeability of the microparticles to water molecules was evaluated by exposing the particles to an atmosphere with 15% relative humidity at 22 °C. For water droplets of the same volume, complete evaporation occurred within 20 s under the same conditions. However, evaporation was slowed down by the ETPTA shells of the microparticles. For a thin ETPTA shell (thickness 5 μm), complete evaporation took about 2 h. Figure 7a shows four images taken after 0, 0.5, 1, and 2 h from the commencement of evaporation. Initially, the shell was spherical, but it buckled in the thinnest area during the evaporation of water. Figure 7b shows the crushed shell after complete evaporation. However, for microparticles with thick shells (15 μm), evaporation proceeded much slower and the particles retained their spherical shape even after the complete evaporation of water. Figure 8a shows images of these microparticles taken after 0, 2, 3, and 6 h of evaporation. An SEM image of a broken shell is shown in Figure 8b. The lack of buckling of the microparticles with thicker shells as the water was evaporated is related to the flexural modulus of the ETPTA shell. Because the modulus is proportional to the cube of the ratio of the shell thickness to the microparticle radius, microparticles with thin shells can be deformed with much greater ease by a decrease in the internal pressure during evaporation compared with microparticles of the same size but with thick shells.

When SCCAs were subjected to external electric fields, the spherical particle geometry and high dielectric constant of water contributed to reducing the electric field inside the shell. Therefore, the electrophoretic movement of the negatively charged particles was inhibited, although the electrophoretic mobility is proportional to the dielectric constant. When we applied an electric field to the core–shell microparticles dispersed in air between two ITO-coated slide glasses separated by 500 μm, where one was grounded and the other was at 100 V, the diffraction color did not change. In fact, the microparticles in air maintained their diffraction color for voltages up to 500 V. For the film-type CCA, 2 V/50 μm (~40 000 V/m) was sufficient to induce particle movement, and the diffraction color was changed by applying an alternating current (AC) electric field with 1 Hz, as shown in Figure S4 and Movie Clip 3 of the Supporting Information. A simple simulation with FEMLAB showed that the electric field is minimized inside the water-filled shell, as shown in Figure 9. For a 100 V difference between two plates separated by 500 μm, the electric field in the core region of the microparticles surrounded by air was just 9138 V/m, which is too small to move the particles. Although the field was 45 690 V/m for 500 V, particle movement was not observed in the experiments, indicating that the electric field in the core region was much reduced in a real situation. In

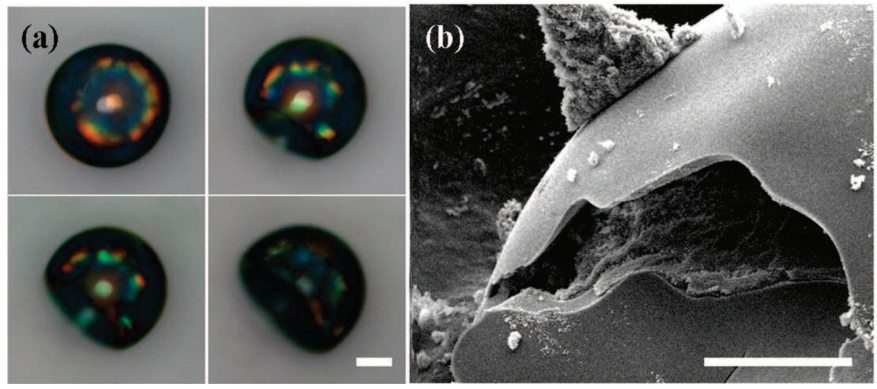

Figure 7. (a) Optical microscope images of SCCA confined in thin ETPTA capsule. The four images were taken after 0 h (top left), 0.5 h (top right), 1 h (bottom left), and 2 h (bottom right) from exposing the particle to an atmosphere that is 15% relative humidity and 22 °C. The shell was deformed from spherical shape due to an evaporation-induced pressure decrease. (b) SEM image of crushed thin shell with 5 μm thickness. The scale bars in (a) and (b) are 100 and 50 μm, repectively.

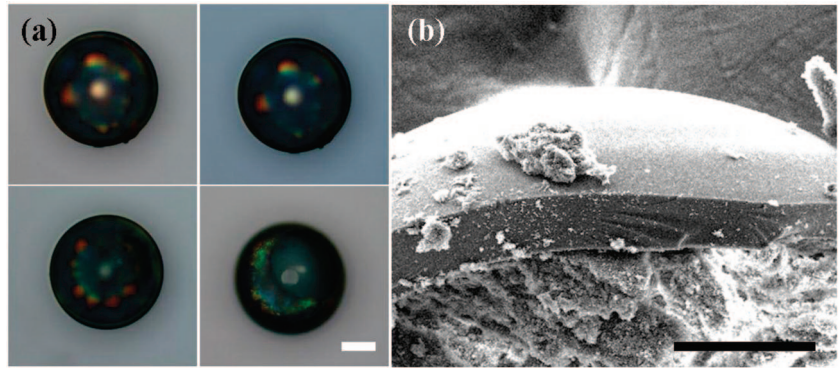

Figure 8. (a) Optical microscope images of SCCA confined in thick ETPTA capsule. The four images were taken after 0 h (top left), 2 h (top right), 3 h (bottom left), and 6 h (bottom right) from exposing the particle to an atmosphere that is 15% relative humidity and 22 °C. The high flexural modulus of the thick shell prevented the shell deformation, and air was infiltrated inside the shell. (b) SEM image of the crushed thick shell with 15 μm thickness. The scale bars in (a) and (b) are 100 and 50 μm, respectively.

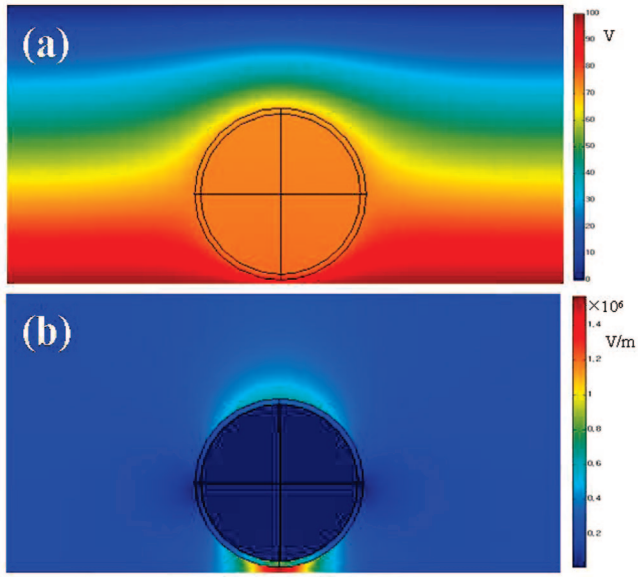

Figure 9. (a) Electric potential and (b) electric field distribution for water core−ETPTA shell microparticles surrounded by air when 100 V was applied as bottom surface separated from grounded top surface by 500 μm.

contrast to an electric field, a magnetic field cannot be screened because of the low magnetic permeability of water, which is similar to that of air. Therefore, a magnetic field may be a useful stimulus for color tuning of CCAs on a fast time scale if the colloids contain a high content of magnetic material.[34a] As reported recently by Ge et al.,[34b] the strength of the magnetic field can modulate the lattice constant, which in turn induces the dynamic color change of the SCCA.

Conclusions

We have demonstrated the self-organization of colloidal microparticles in aqueous media confined in a spherical shell. Using an optofluidic device, we prepared stable double emulsions and solidified the shell emulsion by *in situ* photopolymerization. The fabricated CCA core−polymeric shell microparticles showed particular Bragg diffraction in the visible range, unlike conventional film-type CCAs. Because the crystallization of SCCAs occurs via heterogeneous nucleation at the smooth wall of the spherical emulsion drop, the surface of the core emulsion is the densest (111) plane of fcc lattices. As a result of their spherical symmetry, SCCAs induced photonic band gaps for normal incident light independent of the position on the spherical surface and showed unique color diffraction patterns. On the other hand, the photopolymerized shell has low permeability to water molecules and slowed the evaporation of water molecules by approximately 1000-fold in air. In addition, the shell blocked out the penetration of sodium ions, making it possible to maintain the crystal structure even when the continuous aqueous phase had high ionic strength. Moreover, the spherical geometry of the microparticles and high dielectric constant of the suspension prevented the electrophoretic movement of particles by reducing the electric field inside the shell, thereby stabilizing the CCA structure under high external electric fields. In addition to CCA applications, we believe that the closed shell structure of ETPTA, which affords high chemical resistivity, physical rigidity, and biological stability, will be useful in thermal cycling reactions and encapsulation of toxic materials or biomolecules.

Acknowledgment. This work was supported by a grant from the Creative Research Initiative Program of the Ministry of Education, Science, and Technology for "Complementary Hybridization of Optical and Fluidic Devices for Integrated Optofluidic Systems." The authors also appreciate partial support from the Brain Korea 21 Program and thank Dr. Se-Heon Kim for useful discussion.

Supporting Information Available: Experimental details are described including materials, experimental procedures, and characterization. A few optical microscope and SEM images are also included to demonstrate the high stability of double emulsion and compare with results from the film CCA. In addition, movie clips were edited to show the generation of double emulsion droplets and diffraction color change of film-type CCA under an AC electric field. This material is available free of charge via the Internet at http://pubs.acs.org.

JA800844W